scientific reports

Check for updates

OPEN

Research on an ultrafine water mist partition multistage dust suppression system in underground excavation tunnel

Deji Jing[1,2,4], Qisheng Kan[1,2,4], Mingying Dai[1,3]✉, Jichuang Ma[1,2,4], Chunhua Bao[1,2,4], Pengyu Du[1,2,4] & Ping Chang[5]

A large amount of coal dust is produced in coal mine excavation, which has a serious impact on the working environment and health of underground workers. For this problem, through numerical simulation to understand the temporal and spatial evolution law of coal dust in the excavation tunnel, that is, the coal dust velocity first increases and then decreases along the diffusion direction, and the maximum velocity reaches 8 m/s, and fills the entire tunnel at 50 s. In this regard, the an ultrafine water mist partition multistage dust suppression system was proposed, and numerical simulation studies were carried out on the wind flow distribution and water mist particle transportation law, and the results showed that the air flow velocity in the 0–5 m area was between 6–14 m/s and varied a lot, and the speed of the spray jet in the 10–30 m area decayed faster, and eventually stabilized at 1 m/s. The water mist particles surrounded the cutting head with a speed of 8 m/s in 2 s, and spread to the working face. After 10 s, the water mist particles cover the whole roadway, and the speed is also stabilized at 2 m/s. Through field application and measurement in the I030409 excavation face of Qipanjing Coal Mine, the average reduction efficiency for total dust and respirable dust in the tunnel reached 91.74% and 93.4%, respectively, which effectively controls the problem of dust pollution in the excavation tunnel.

Keywords Tunnel excavation, Coal dust control, Wet dust removal, Migration law, Numerical simulation, Partition governance

With the development of the global economy, the demand for various energy sources worldwide is increasing. Although the new energy technologies are developed, coal, as a basic energy source, plays a vital role[1–4]. According to the 2024 Statistical Review of World Energy, the world's total coal production in 2023 reached 90.957 billion tons (179.24 EJ), an increase of 3.1% over that in 2022, and global production exceeded 9 billion tons for the first time[4]. China's total coal output reached 4.71 billion tons, accounting for 51.8% of the world's total coal output. As the world's largest coal production country, China's research and development of mechanized coal equipment has become increasingly intensive. With the wide application of new technology and new materials, the way in which underground workers are exposed to dust in occupational activities has become increasingly complex and diverse, which seriously endangers the health of underground workers[5–10]. According to statistics, the incidence of occupational diseases in China is the highest in the world and is approximately 10 times greater than that in developed countries. Figure 1 shows the number of occupational diseases and the proportion of pneumoconiosis cases in China from 2016 to 2023. Pneumoconiosis cases decreased from 27,992 to 8,051 from 2016 to 2023. Although there is a downward trend as a whole, the number of newly diagnosed occupational disease cases and cases of pneumoconiosis still remain at a high level[11–14]. Notably, high concentrations of dust directly or indirectly lead to the occurrence of underground explosion accidents and fire accidents, causing considerable economic losses to coal mining enterprises and society[15].

[1]College of Safety Science and Engineering, Liaoning Technical University, Fuxin 123000, Liaoning, China. [2]Key Laboratory of Mine Thermo-motive Disaster and Prevention, Ministry of Education, Fuxin 123000, Liaoning, China. [3]Aerospace Information Software Technology Co., Ltd, Beijing 100000, China. [4]Erdos Research Insititute L.N Technical University, Liaoning Technical University, Ordos 017000, Inner Mongolia, China. [5]WA School of Mines: Minerals, Energy and Chemical Engineering, Curtin University, Kalgoorlie, WA 6430, Australia. ✉email: 1432244912@qq.com

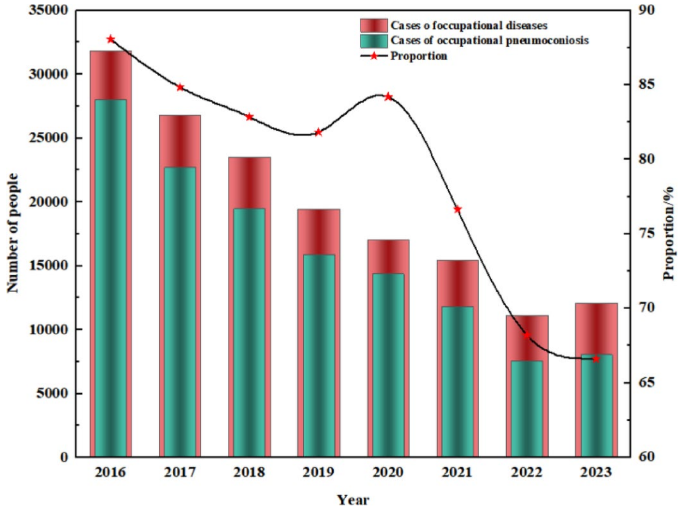

Fig. 1. Occupational diseases and pneumoconiosis statistics from 2016 to 2023.

In summary, reducing the dust concentration in tunnel during the coal mine excavation process is an urgent problem. There are two main components of the dust pollution problem in excavation tunnel. First, due to the increase in the degree of mechanization of coal mines, a large force is needed in the excavation process, which leads to greater kinetic energy when dust in the excavation workface is generated. Second, the airflow in excavation tunnel is complex, and dust is difficult to capture[16–19]. Common dust reduction methods include wet and dry dust reduction, and spray dust reduction is the simplest and most effective method of wet dust reduction; thus, most coal mines use spray dust reduction[20–24]. At present, many scholars worldwide have conducted in-depth research on the dust migration law and spray dust reduction technology in excavation tunnel.

For example, Hu et al.[25] used a numerical simulation method to study the dust diffusion characteristics of the continuous dust release period (CRP) and stop dust release period (SRP) and obtained the migration law of dust in the driving area of a tunneling machine during the CRP and SRP. Nie et al.[27–28] used numerical simulation to analyze the coupling diffusion law of airflow, gas, and dust in excavation tunnel under long-pressure and short-pumping ventilation conditions and explored the best position of an exhaust pipe through experiments. The above research has analyzed and summarized the coal dust transport law in the excavation tunnel, which provides a theoretical basis for the management of coal dust in the excavation tunnel. Zhou et al.[29] conducted a numerical simulation study on the coupling diffusion law of coal dust and rock dust during the excavation of coal-rock mixed tunnel and reported that the diffusion law of coal dust and rock dust conforms to the linear equation $L_D = 0.82\ T + 11$. They proposed cloud-mist dedusting technology to solve the dust pollution problem, and the dust removal efficiency reached more than 75% after field application. On the basis of the theory of fluid mechanics, Zhang et al.[30] conducted numerical simulation calculations on the airflow-dust field and airflow-droplet field in excavation tunnel, obtained the distribution law of dust and droplets, and studied the effect of multistage atomization The above researches have put forward different management programs for the coal dust transportation law in the roadway and carried out on-site application, which provides technical support for the coal dust management in the roadway.

Although existing research has played an important role in dust reduction in excavation tunnel, the internal space of excavation tunnel is already limited, more mechanical equipment is installed, which affects the workers ability to complete their work, and a variety of dust control methods affect each other and sometimes have side effects. Therefore, on the basis of spraying dust reduction, this study proposes an ultrafine water mist partition multistage dust suppression system, which captures and settle the coal dust generated by tunneling through the cutting head atomizer device, and then collects and purifies it through the wet dust removal fan; and the coal dust escaping to the back of the excavation tunnel is further blocked by the two full cross-section spraying devices, realizing the effect of zoned step-by-step dust reduction.

Mathematical model
Turbulent flow model
The airflow in the excavation tunnel is incompressible, so the Reynolds-averaged Navier–Stokes equations can be used to calculate it[31]. The airflow in the excavation tunnel in this study is a turbulent flow with a large Reynolds number, so the Spalart–Allmaras model, the standard k-ε model and the k-ω model can be selected for calculation. Among them, the standard k-ε model performs better in terms of calculation accuracy and calculation time than the other two models do[32]. Therefore, the standard k-ε model is selected for simulation calculation, and the control equation is as follows[33]:

$$\rho \frac{\partial k}{\partial t} + \rho u \cdot \nabla k = \nabla \left[\left(\mu + \frac{\mu_T}{\sigma_k} \right) \nabla k \right] + P_k - \rho \varepsilon \tag{1}$$

$$\rho\frac{\partial\varepsilon}{\partial t}+\rho u\cdot\nabla\varepsilon=\nabla\left[\left(\mu+\frac{\mu_T}{\sigma_\varepsilon}\right)\nabla\varepsilon\right]+C_{\varepsilon1}\frac{\varepsilon}{k}P_k-C_{\varepsilon2}\rho\frac{\varepsilon^2}{k} \tag{2}$$

Generating item:

$$P_k=\mu_T\left[\nabla u:(\nabla u+(\nabla u)^T)-\frac{2}{3}(\nabla\cdot u)^2\right]-\frac{2}{3}\rho k\nabla\cdot u \tag{3}$$

Turbulent viscosity:

$$\mu_T=\rho C_\mu\frac{k^2}{\varepsilon} \tag{4}$$

where ρ is the fluid density, kg/m^3; k is the turbulent kinetic energy, J; u is the fluid velocity, m/s; μ is the gas dynamic viscosity; μ_T is the turbulent viscosity coefficient; σ_k and σ_ε are the turbulent kinetic energy k and the dissipation rate ε, respectively; ε is the turbulent dissipation rate; and p is the pressure, Pa. The experimental constants are $c_\mu=0.09$, $\sigma_k=1$, $\sigma_k=1.3$, $c_{\varepsilon 1}=1.44$, and $c_{\varepsilon 2}=1.92$.

Particle tracing model

Particle tracing for the fluid flow model is selected for the numerical simulation of coal dust particles and water mist particles in excavation tunnel[34]. The model is based on the motion equation of Newton's second law for simulation calculations. It can define a variety of particle properties and release methods and finally calculate the migration trajectory of particles. Since the coal dust in the excavation tunnel belongs to a kind of dilute particle flow, it is also necessary to add the Stokes drag model[35]. The particle motion equation is as follows:

$$\frac{d}{dt}(m_p v)=\sum F \tag{5}$$

Stokes' drag equation:

$$F_D=\frac{1}{\tau_p}m_p(u-v) \tag{6}$$

$$\tau_p=\frac{4\rho_p d_p^2}{3\mu C_D \mathrm{Re}} \tag{7}$$

$$C_D=\frac{24}{Re}(1+0.15Re^{0.687}) \tag{8}$$

$$\mathrm{Re}=\frac{\rho\left|u-v\right|d_P}{\mu} \tag{9}$$

where m_p is the particle mass, kg; ΣF is the sum of the forces acting on the particle, N; F_D is the drag force, N; τ_p is the shear stress, N; C_D is the drag coefficient; Re is the Reynolds number; u and v are the airflow velocity and particle velocity, respectively, m/s; ρ_p is the particle density, kg/m^3; d_p is the particle diameter, μm; and μ is the gas dynamic viscosity, Pa·s.

Geometric model and boundary conditions

Geometric model

In the numerical simulation, the closer the geometric model is to the field situation, the more realistic the simulation results[36]. Therefore, to ensure the accuracy of the numerical simulation, according to the actual measurement size of the I040901 excavation workface in the Qipanjing Coal Mine, COMSOL software is used for 1:1 geometric modeling, as shown in Fig. 2. The compressed air side of the tunnel is defined as the right side, and the return air side is defined as the left side. Taking the lower left side of the tunnel as the origin of the model, the x-axis is established along the direction of the compressed air side of the tunnel, the y-axis is established along the direction opposite the excavation direction, and the z-axis is established along the direction from the tunnel floor heave to the tunnel roof. The geometric model of the excavation tunnel is composed of an EBZ200 cantilever tunneling machine, a pressurized air duct, a KCS-450 wet dust removal fan, a belt conveyor, a full cross-section atomizer device and a cutting head atomizer device. For the excavation tunnel, the length is 40 m, the cross-sectional width is 5 m, and the peak height is 3.8 m; the air duct has a length of 35 m and a diameter of 1 m, and it is located at the top of the tunnel and is 5 m from the workface. The wet dust removal fan is set on the tunneling machine and is connected with an air duct with a diameter of 0.8 m, and the suction port is 3 m from the workface. The belt conveyor is connected with the tunneling machine. There are two full cross-section atomizer devices 15 m and 30 m behind the workface and 3 m from the tunnel floor heave.

Mesh division and independence test

The number of meshes and the quality of the elements play crucial roles in the simulation process, which determines the accuracy and time of the simulation[37]. When meshing, it is necessary to select the appropriate number of meshes and element quality. When the number of meshes is too large, the calculation time will be

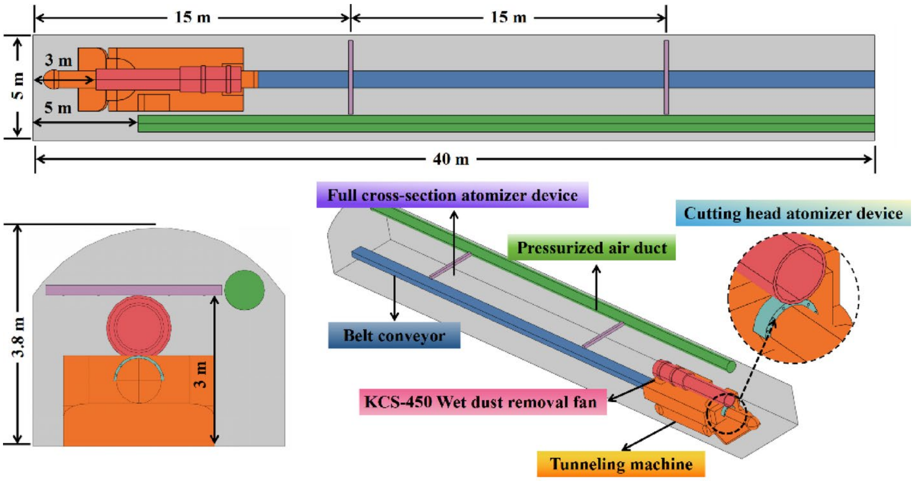

Fig. 2. Geometric model.

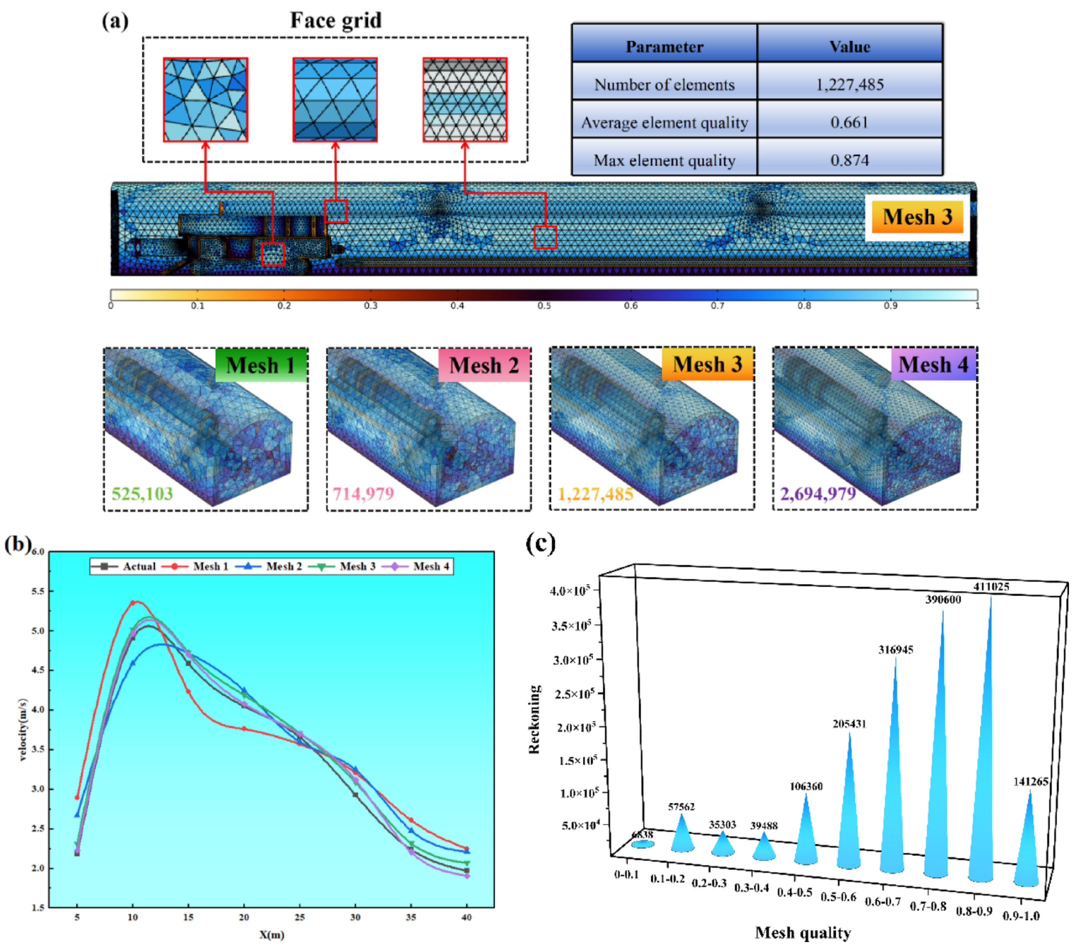

Fig. 3. Grid independence test.

too long, but the corresponding calculation accuracy will be greatly improved[38]. Therefore, grid independence verification is required before simulation to save time and ensure accurate calculations.

Using the meshing function of COMSOL software, four different mesh structures were obtained as shown in Fig. 3 with mesh counts of 525,103, 714,979, 1,227,485, and 2,694,979. Since the diffusion of coal dust is affected mainly by the air flow, the air velocity is selected as the research target to verify the independence of the mesh. The velocity distributions under four different grid structures were intercepted at the height of the breathing

Speed (m/s)	Distance (m)							
	5 m	10 m	15 m	20 m	25 m	30 m	35 m	40 m
Actual	2.18	4.91	4.59	4.05	3.66	2.93	2.24	1.97
Mesh 1	2.89	5.35	4.23	3.76	3.57	3.21	2.61	2.25
Mesh 2	2.67	4.59	4.72	4.25	3.60	3.25	2.48	2.21
Mesh 3	2.31	5.02	4.73	4.19	3.71	3.09	2.32	2.07
Mesh 4	2.23	4.97	4.70	4.08	3.70	3.12	2.21	1.91

Table 1. Comparison of actual simulated air velocity at different distances.

Type	Project	Parameter settings
General	Solver type	Stationary/Time-dependent
	Gravity	Z:-g
Boundary conditions	Entrance boundary condition	Inlet velocity
	Inlet velocity (m/s)	17
	Export boundary condition	Outlet pressure
Turbulent flow, k-ε	Fluid density (kg/m^3)	1.2
	Dynamic viscosity (Pa·s)	1.79×10^{-5}
	Diffusion coefficient of a gas molecule (m^2/s)	2×10^{-5}
	Temperature (K)	293.15
	Wall setting	No slip
Particle tracing for fluid flow	Liquid droplet density (kg/m^3)	1.0
	Liquid droplet surface tension (N/m)	7.29×10^{-2}
	Nozzle flow rate (ml/min)	110
	Atomised semi-angle (degrees)	30
	Density of dust sources (kg/m^3)	1.65×10^{-3}
	Average particle mass (kg)	5×10^{-12}
	Standard deviation of particle mass (kg)	1×10^{-11}
	Turbulent dispersion model	Continuous random walk
	Wall condition	Freeze
	Solid particle density (kg/m^3)	2.1

Table 2. Boundary conditions and parameter settings.

zone in the centre of the tunnel and compared with the actual airflow velocities in the field, and the results are shown in Fig. 3b and the specific data are shown in Table 1. From the figure and table, it can be seen that the trend of the velocity changes under the four grids is basically the same, but the airflow velocity of Mesh 1 and Mesh 2 fluctuates greatly in the range of 5–40 m, while the airflow velocity of Mesh 3 and Mesh 4 is closer to the actual airflow velocity and the difference is smaller. Therefore, choosing Mesh 3 for the numerical simulation meets the accuracy requirements, and continuing to increase the number of grids will increase the computational cost. Further grid quality counts are performed for Mesh 3. As shown in Fig. 3c, the cell counts are highest in the cell quality range of 0.6 to 0.8, the minimum and average cell masses are 0.005 and 0.661, respectively, which satisfy the requirements of simulation.

Boundary conditions and parameter settings of the numerical simulation
According to the actual situation of the excavation tunnel, the relevant boundary parameters are set, and the COMSOL built-in solver is used for simulation calculations. According to the on-site measurement, the air volume supplied by the pressurized wind pipe of the tunnel is 500 m^3/min, and the coal dust with a particle size of 80 μm accounts for 80% of the total. The outlet of the pressurized air duct and the wet dust removal air is set as the speed inlet, and the outlet is set as the pressure outlet. The settings of the specific boundary parameters are shown in Table 2.

Numerical simulation analysis
Analysis of the airflow field and particle field under different conditions
By understanding the airflow field and coal dust particle field under different ventilation conditions in the excavation tunnel, a targeted dust reduction scheme can be proposed. Figure 4 shows the airflow streamline diagram of the wet dust removal fan under different conditions. In the figure, the streamline represents the airflow trajectory, the color represents the airflow velocity, and the arrow represents the airflow direction. The specific analysis is as follows:

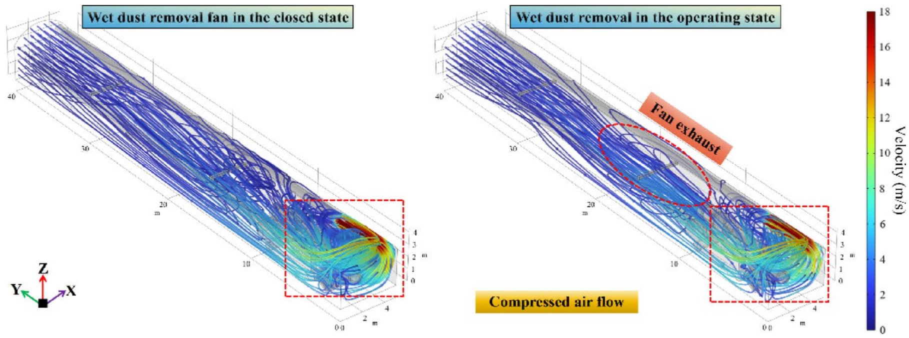

Fig. 4. Spatial distribution of the airflow streamline diagram under different ventilation conditions.

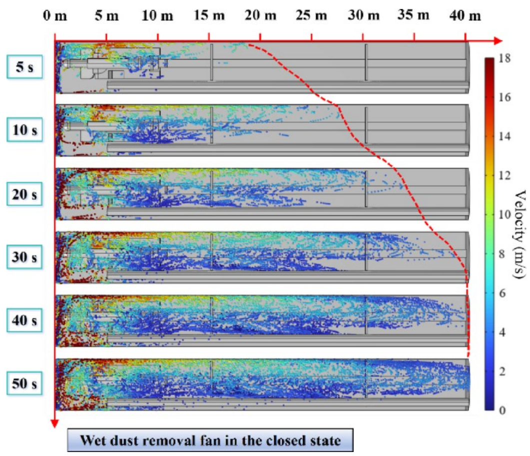

Fig. 5. Diagram of the spatiotemporal diffusion of coal dust in the dust removal fan closed state.

(1) When the wet dust removal fan is not open, the speed changes greatly in the range of 0–10 m, and the speed is 8–17 m/s, which is affected mainly by the pressurized air duct. The air flow from the compressed air duct hits the working face and then is offset. Under the combined action of the obstruction of the roadheader and the negative pressure of the compressed air duct, some airflow forms an eddy current near the cab. However, most of the airflow moves backward with the return air of the roadway. Because there is only a pressure air duct in the roadway, the airflow diffusing backward is not affected by other airflows, and the airflow velocity is stable at approximately 1 m/s.
(2) When the wet dust removal fan is open, the position of the area where the speed changes greatly is the same as that when it is not open. Owing to the opening of the fan, part of the airflow is affected by suction and enters the air duct. At the same time, the airflow velocity is 4 m/s at the outlet of the fan, and the air moves backward along the roadway. In addition, the airflow is affected by the negative pressure of the pressure air duct and forms an eddy current at 15 m on the pressure air side. Compared with the unopened position, it is farther from the cab, which prevents the eddy currents that form near the cab from accumulating dust particles.

The temporal and spatial evolution laws of coal dust during the excavation process are explored, and the dust migration law in different states and at different time scales is analyzed to propose a corresponding spray dust isolation method. Figures 5 and 6 show the distributions of coal dust in the unopened and open states of the dust removal fan, respectively. The spheres in the figure represent the coal dust particles, and the color represents their migration speed.

Combined with the analysis of the airflow field, the following rules are obtained:

(1) At 5 s, the coal dust near the cutting head is affected by airflow blowing from the pressurized air duct and rapidly diffuses 18 m along the return air side of the tunnel. The velocity first increases and then decreases along the diffusion direction, and the maximum velocity reaches 8 m/s at 5 m.
(2) At 10 s, the coal dust as the air flow spreads to 27 m, and the migration trend of the coal dust is the same as that at 5 s; however, in the range of 7–15 m, some coal dust diffuses to the compressed air side and accumulates above the tunneling machine at a lower speed (1 m/s), but no high-concentration coal dust group forms. Moreover, a small amount of coal dust also accumulates near the cab of the tunneling machine.

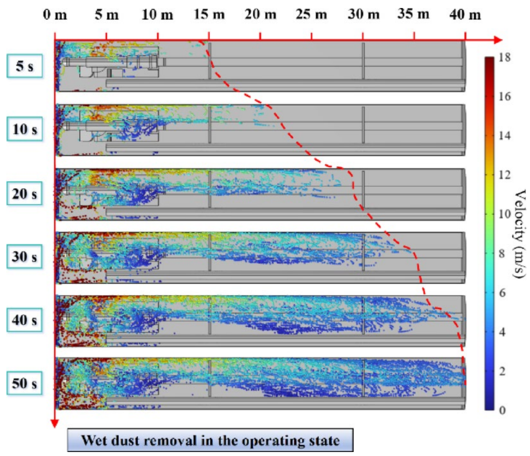

Fig. 6. Diagram of the spatiotemporal diffusion of coal dust in the dust removal fan operating state.

(3) At 20 s, a large amount of coal dust gathers near the cutting head. Driven by the continuous airflow, the coal dust on the return air side diffuses to 34 m, and the part of the coal dust that diffuses to the compressed air side diffuses to the rear of the tunnel to 27 m. At this time, a large amount of dust gathers above the tunneling machine and the belt.
(4) At 30 s, the coal dust completely covers the cutting head and basically spreads to the tail of the tunnel. At 50 s, the coal dust fills the entire tunnel. At this time, the coal dust in the rear section of the pressure air side shifts to the return air side because of the influence of the airflow, and this part of the coal dust is basically stable at the tail of the tunnel.

From Fig. 6, the following coal dust particle migration law is obtained:

(1) At 5 s, part of the coal dust is pumped away by the dust removal fan, the movement trend of the remaining coal dust is consistent with that when the fan is not open; however, its diffusion trend is obviously curbed, and the diffusion distance is significantly shortened to 14 m. At this time, there is some coal dust on the right side of the cutting head, and there are basically no coal dust particles on the left side.
(2) At 10 s, the coal dust is affected by the air flow movement and spreads 20 m along the return air side. A small part of the coal dust in the range of 5–10 m diffuses to the compressed air side at a speed of 1 m/s, and the amount of coal dust near the cab is significantly reduced by the traction of the fan compared with that of the unopened fan.
(3) At 20 s, the coal dust diffuses to 28 m under the continuous airflow, and there is only a small amount of coal dust behind the tunneling machine, which is caused by the combined action of the fan and the compressed air duct. Compared with that of the unopened fan, the diffusion trend of the coal dust in the range of 10–25 m is obviously curbed.
(4) At 30 s, the coal dust diffuses to 35 m, and the coal dust on the return air side diffuses to the compressed air side at a speed of 1 m/s. Coal dust fills the tunnel in 50 s. However, unlike the case with the fan unopened, the coal dust does not gather in the 10–20 m area, and the amount of coal dust is significantly reduced by the traction of the fan after 15 m.

Analysis of the law of airflow in an ultrafine water mist partition multistage dust suppression system

By analyzing the airflow streamline in the excavation tunnel and the airflow velocity on different ZX cross-sections, the airflow migration law of the ultrafine water mist partition multistage dust suppression system in the closed space of the tunnel is obtained. The three-dimensional spatial distribution of the airflow streamline is shown in Fig. 7. The streamline in the diagram indicates the airflow trajectory, the arrow indicates the direction of the airflow vector, and the color gradient indicates the airflow velocity. The specific analysis is as follows:

(1) The area with a large velocity change is mainly between 0–10 m, which is affected by the pressure air duct, wet dust removal fan and cutting head atomizer device. At the same time, the velocities of the two full cross-section atomizer devices (15 m and 30 m) also changed significantly, but the airflow velocity attenuated rapidly, and the airflow velocity was basically stable at 1 m/s after 2 m.
(2) The high-speed airflow ejected from the air duct impacts the workface, forming a high-speed flow field of 6–18 m/s in the range of 5 m. When the high-speed airflow collides with the working face, its momentum drops sharply, and a flow field of approximately 6 m/s forms at the bottom of the return air side. The suction outlet of the fan inhales part of the airflow, and at the same time, a flow field area of 6 m/s forms at the exhaust outlet of the fan.
(3) The cutting head atomizer device ejects high-speed air flow to wrap the cutting head. The air flow deflects upward and quickly covers the whole working face, which is affected by the suction port of the fan. Full cross-section atomizer device #1 and #2 also shoot high-speed air in the direction of the tunnel floor. When

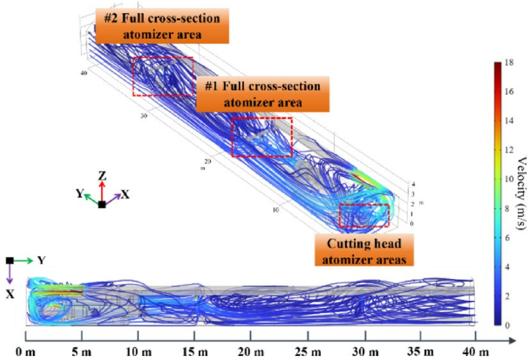

Fig. 7. Spatial distribution of the airflow streamline diagram of the dust suppression system.

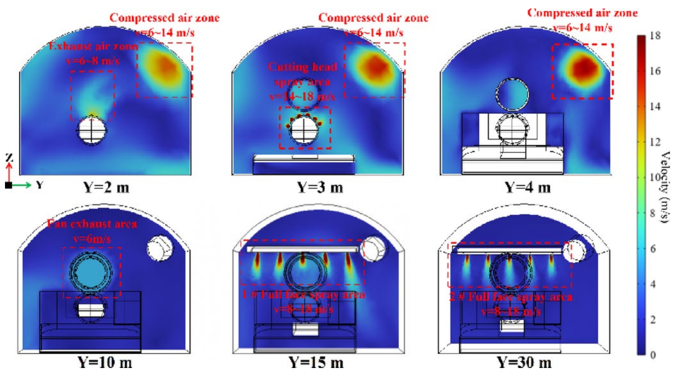

Fig. 8. Cross-sectional views of the velocity at different positions in the y-axis direction.

it collides with the tunnel floor, its speed suddenly decreases and stabilizes at approximately 1 m/s, and it migrates to the rear of the tunnel.

The streamline diagram shows that the airflow migrating from the workface to the back is divided into two main parts. To further study the airflow migration law inside the tunnel, velocity section cloud images at different positions are intercepted along the Y-axis, as shown in Fig. 8. The color in the figure represents the airflow velocity. The area with a velocity greater than 6 m/s is the high-speed area, the area with a velocity of 2–6 m/s is the medium-speed area, and the area with a velocity less than 2 m/s is the low-speed area. Combined with the streamline diagram, the change in airflow velocity inside the tunnel is analyzed. The specific analysis is as follows:

(1) According to the velocity section cloud images at Y = 2 m, 3 m and 4 m, there is a high-speed area of 6–14 m/s in the upper right corner of the tunnel, and the cutting head area is surrounded by a high-speed area of 16 m/s. After the airflow collides with the workface, offset occurs, and a high-speed area of 6 m/s is formed on the right side of the bottom of the tunnel and the return air side. There is also a high-speed area of 6 m/s at the suction port of the fan.
(2) According to the velocity section cloud images at Y = 10, 15, and 30 m, the airflow velocity inside the tunnel basically remains stable at approximately 2 m/s, whereas at Y = 10 m, a high-speed area of 6 m/s is observed in the fan outlet area. Moreover, at Y = 15 m and 30 m, airflow with a velocity of 18 m/s is sprayed from the direction of the tunnel floor by the full cross-section atomizer device, but its speed is suddenly reduced and stabilized at 1 m/s.

Analysis of the law of water mist particles in an ultrafine water mist partition multistage dust suppression system

The three-dimensional spatial distribution of water mist particles at different times can be intercepted, as shown in Fig. 9. The points in the figure represent the position of the water mist particles, and the color represents the velocity of the water mist particles. Combined with the distribution of airflow streamlines, the migration law of water mist particles is analyzed. The results are as follows:

(1) At 2 s, the water mist particles surround the cutting head, have a large momentum, and diffuse to the workface at a speed of 8 m/s. Full cross-section atomizer device #1 is affected by the exhaust air of the dust removal fan, the water mist particles diffuse to the rear of the tunnel at a speed of 6 m/s, and the range reaches 9 m. Full cross-section atomizer device #2 is less affected by fan exhaust than #1 and diffuses backward at a speed

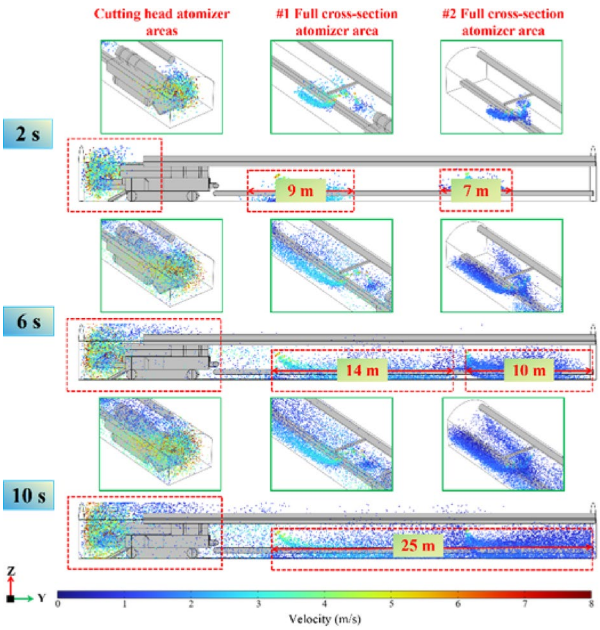

Fig. 9. Diagram of the spatiotemporal diffusion of water mist particles.

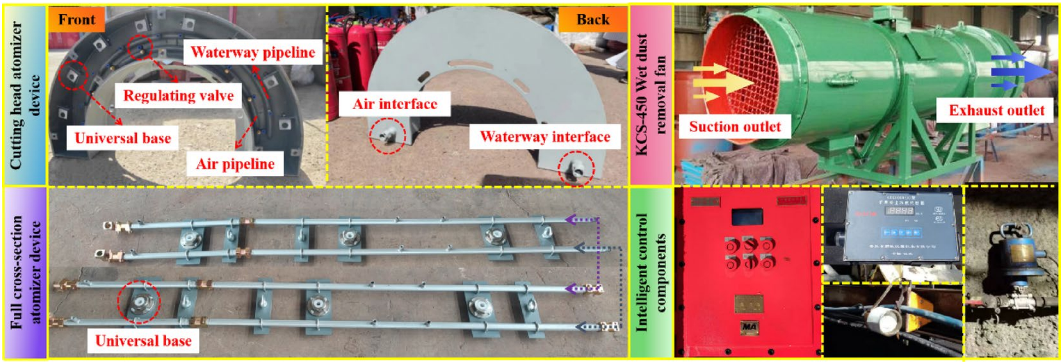

Fig. 10. Components of the ultrafine water mist partition multistage dust suppression system.

of 4 m/s, and the range reaches 7 m. At the same time, the water mist particles above the tape shift backward after hitting the tape, but the diffusion range is short.

(2) At 6 s, the workface is basically covered by water mist particles. Some water mist particles are inhaled by the fan after they hit the workface, and some water mist particles diffuse along the lateral rear of the return air of the tunnel. The water mist particles generated by full cross-section atomizer device #1 diffuse to the bottom of the tunnel and completely cover the belt conveyor, and the diffusion range reaches 14 m. The migration trend of the water mist particles generated by full cross-section atomizer device #2 is basically the same as that of #1, but the diffusion range is short, at 10 m.

(3) At 10 s, many water mist particles accumulate near the cutting head to capture and settle the coal dust generated during tunneling. At the same time, some water mist particles gather on the return air side and spread to the rear of the tunnel, and the speed is stable below 2 m/s; the water mist particles produced by the full cross-face spray completely cover the tape, and a water mist particle film is formed to prevent the diffusion of coal dust particles on the tape. Moreover, the water mist particles generated by the full cross-section spray form two fog curtains, which effectively block dust diffusion.

Field application of an ultrafine water mist partition multistage dust suppression system

Research and development of dust removal systems

The developed ultrafine water mist partition multistage dust suppression system is composed of a supersonic aerodynamic atomization device (including a full cross-section atomizer device and a cutting head atomizer device) and wet dust removal fan and intelligent control components (including a PLC control box, a dust concentration sensor, an infrared sensor and an electromagnetic ball valve), as shown in Fig. 10. The nozzle used

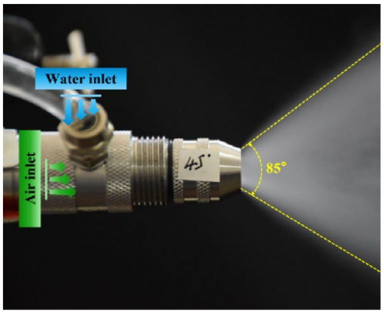

Fig. 11. Supersonic water suction aerodynamic atomization nozzle.

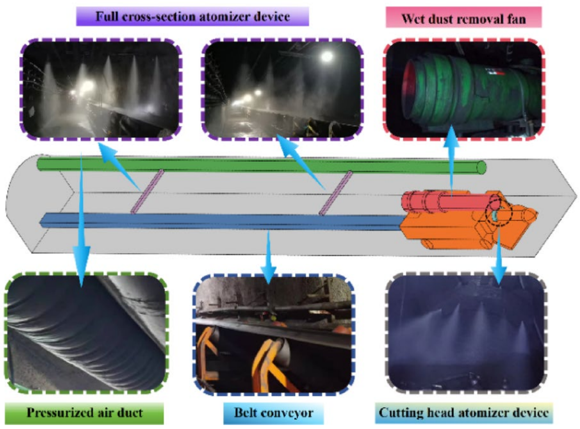

Fig. 12. Field application of an ultrafine water mist partition multistage dust suppression system.

in the atomizing device is a supersonic water suction aerodynamic atomization nozzle, as shown in Fig. 11. The nozzle is based on the principle of supersonic atomization, that is, the jet atomization process in a supersonic airflow. Using its internal Laval tube structure to form a supersonic flow field, under the action of high-speed shear airflow, so that the liquid at the beginning of entering the flow field will be able to achieve the effect of micron-sized droplets. Because the supersonic airflow in its nozzles is a controlled, continuous flow, the energy is primarily used to atomise and drive the droplets into motion, so no damaging shockwaves are formed[39]. The nozzle probe has a diameter of 0.8 mm. At a pneumatic pressure of 0.4 MPa, its range can reach 3.8 m, and the atomization angle can reach 85°. The air and water consumption reached 4.2 m^3/h and 93.3 ml/min, respectively.

Field application verification

According to the actual situation of coal dust generation in the I040901 excavation workface of the Qipanjing Coal Mine[40], the ultrafine mist multistage partition dust reduction system is reasonably arranged, as shown in Fig. 12. The cutting head atomizer device is set at the cantilever of the tunneling machine, the wet dust removal fan is set on the body of the tunneling machine, and the full cross-section atomizer device arranges 15 m and 30 m from the working face.

The velocity distribution along the line from the point (4.5, 0, 1.5) to the point (4.5, 40, 1.5) in the excavation tunnel when the spray dust suppression system is turned on is intercepted and compared with the actual velocity on-site when the spray dust suppression system is activated, as shown in Fig. 13. The area from 0 to 10 m is the working face spray area, the area from 10 to 25 m is the #1 full section spray area, and the area from 25 to 40 m is the #2 full section spray area. Since the water mist particles diffuse under the entrainment of the roadway air flow, by comparing the simulated and actual roadway air flow velocities, the diffusion law of the water mist can be inferred.

By observing the comparison diagram of the spray situation and the air flow in the excavation tunnel, it can be known that in the area of 0–10 m, due to the influence of the air flow blown out by the pressure air duct, the velocity is relatively high. Therefore, the water mist particles generated by the cutting head spray device have high kinetic energy under the action of the air flow. These particles can quickly envelop the cutting head, reducing the outward escape of dust. They can also cover the entire working face, capturing and settling the coal dust generated during the roadway driving. Meanwhile, under the negative pressure of the wet dust removal fan, the water mist particles entrain the dust and move towards the air inlet of the fan, capturing and filtering the dust that has been settled by the spray of the cutting head spray device, thus reducing the diffusion of dust into the excavation tunnel. In the area of 0–25 m, under the action of the #1 full section spray, the water mist particles

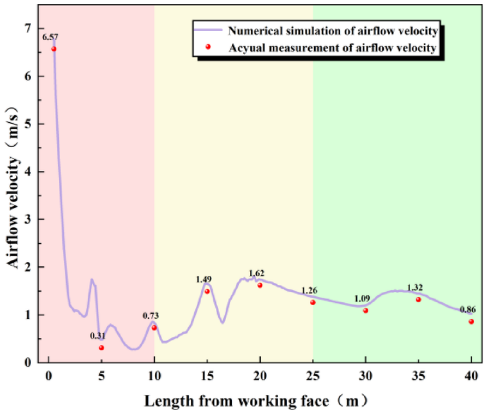

Fig. 13. Comparison between simulated and actual wind speed in the excavation tunnel.

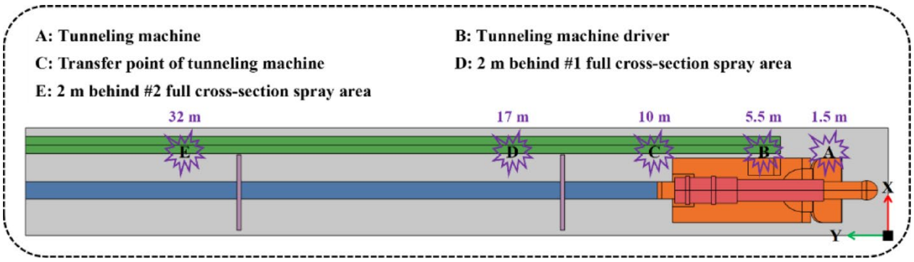

Fig. 14. Locations of the measuring points.

are radially sprayed in a conical shape onto the surface of the tunnel floor and the belt conveyor. Affected by the air flow at the outlet of the fan, there is a distinct tendency for the water mist particles to diffuse towards the rear of the roadheader. At the transfer point behind the roadheader, the high-speed water mist particles generated there block the coal dust, preventing it from diffusing towards the rear. In the area of 25–40 m, the velocity distribution shows little difference from that in the area of 10–25 m, which is consistent with the on-site water mist distribution. Since the spray section in this range is relatively far from the outlet of the fan, the influence of the air flow is significantly weakened, effectively isolating the diffusion of coal dust on the surface of the belt conveyor caused by the action of the air flow.

In summary, the application of the ultrafine water mist partition multistage dust suppression system successfully divided the tunnel into three areas, realizing the effect of zoned step-by-step dust reduction, which is consistent with the simulation results of the spray dust reduction system and further illustrates the effectiveness of the ultrafine water mist partition multistage dust suppression system.

To measure the dust reduction efficiency of the ultrafine water mist partition multistage dust suppression system, the AKFC-92A dust sampler was used to measure the dust concentration at different locations along the excavation tunnel[41], and the arrangement location is shown in Fig. 14. Five dust sampling points were arranged at the center of the excavation tunnel sidewalk ($X = 4.2$ m) along the height of the breathing zone ($Z = 1.6$ m), which were the cutting head of the tunneling machine ($Y = 1.5$ m), the driver's cab of the tunneling machine ($Y = 5.5$ m), the transfer point after the tunneling machine ($Y = 10$ m), the rear of the #1 full cross-section spray ($Y = 17$ m) and #2 full cross-section spray ($Y = 32$ m). The most accurate dust sampling-drying-weighing method was also used to measure the total and respirable dust concentrations before and after dust reduction to prevent moisture in the air from affecting the measurement results. The results of the field measurements are shown in Fig. 15, the average dust reduction efficiencies of total dust and respirable dust are 91.74% and 93.4%, respectively.

Conclusion

In this study, to address the serious pr1oblem of coal dust pollution in the I030409 excavation workface of the Qipanjing Coal Mine, COMSOL software is used to simulate the distribution of air flow and the temporal and spatial evolution of coal dust in the tunnel via numerical simulation, and according to the simulation results, a scheme for an ultrafine water mist partition multistage dust suppression system is proposed. Moreover, the numerical simulation method is used to calculate the airflow distribution of the dust removal system and the temporal and spatial evolution laws of the water mist particles to verify the effectiveness of the ultrafine water mist partition multistage dust suppression system. The following conclusions are reached:

(1) The airflow distribution when the dust removal fan is turned on is roughly the same as that when it is not turned on. The maximum air velocity can reach 17 m/s, and it gradually decreases to 1 m/s after it collides

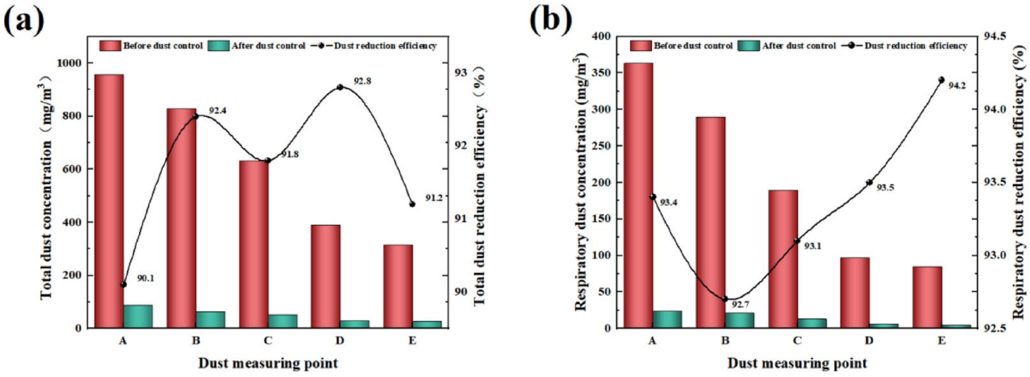

Fig. 15. Rates of (**a**) total dust reduction and (**b**) respiratory dust reduction.

with the workface. The difference is that the vortex appears at 15 m on the compressed air side. The velocity of coal dust first increases and then decreases along the diffusion direction, the maximum velocity reaches 8 m/s, and the whole tunnel is filled at 50 s.

(2) The airflow distribution of the dust removal system in the tunnel is more complex. A high-speed zone of 6–18 m/s forms within 5 m from the working face, and the speed gradually decreases to 1 m/s. However, a high-speed zone of 6 m/s appears at the outlet of the dust removal fan. Moreover, the airflow velocity in the full cross-section spray area decreases from 18 m/s to 1 m/s.

(3) The water mist particle field shows that the water mist particles from the cutting head cover the whole working face with a speed of 8 m/s in 2 s. After 10 s, the roadway is covered by the water mist particles under the effect of two full-section sprays, and its speed is also stabilized at 2 m/s. Successfully dividing the roadway into three zones, and realizing the effect of zoned step-by-step dust reduction.

(4) After the application of the new dust reduction system in the I030409 excavation workface of the Qipanjing Coal Mine, the average reduction efficiency for total dust and respirable dust reached 91.74% and 93.4%, respectively. The ultrafine water mist partition multistage dust suppression system realizes the partitioning and the step-by-step treatment of coal dust in tunnel.

Data availability

All data generated or analysed during this study are original and are included in this published article.

Received: 30 October 2024; Accepted: 22 April 2025
Published online: 28 April 2025

References

1. Nie, W. et al. Optimization of wind-and-water coordinated dust reduction device for coal mine return airway based on CFD technology. *Powder Technol.* https://doi.org/10.1016/j.powtec.2024.119932 (2024).
2. Lu, Y. et al. Study on air curtain cooperative spray dust removal in heading face based on swirl theory. *J. Environ. Chem. Eng.* **10**(6), 108892. https://doi.org/10.1016/j.jece.2022.108892 (2022).
3. Zhou, W. et al. A novel method for reducing the amount of dust produced by roadheaders based on the numerical simulation of coal breakage. *Fuel* **343**, 127978. https://doi.org/10.1016/j.fuel.2023.127978 (2023).
4. Wu, W. et al. Failure characteristics and cooperative control strategies for gob-side entry driving near an advancing working face: A case study. *Processes* **12**(7), 1398 (2024).
5. Zhou, G. et al. Study on the characteristics of compound dust source pollution and foam dust suppression technology in coal mine anchor excavation production. *Process Saf. Environ. Prot.* **186**, 593–611. https://doi.org/10.1016/j.psep.2024.03.119 (2024).
6. Din, I. U. et al. Heavy metal (loid) s contamination and ecotoxicological hazards in coal, dust, and soil adjacent to coal mining operations, Northwest Pakistan. *J. Geochem. Explor.* **256**, 107332. https://doi.org/10.1016/j.gexplo.2023.107332 (2024).
7. Xu, C. et al. Construction of an occupational-dust hazard testing platform: An experimental study on the deposition mechanisms. *Adv. Powder Technol.* **34**(6), 104027. https://doi.org/10.1016/j.apt.2023.104027 (2023).
8. Shangguan, Y. et al. Physicochemical characteristics and oxidative potential of size-segregated respirable coal mine dust: Implications for potentially hazardous agents and health risk assessment. *Int. J. Coal Geol.* **282**, 104433. https://doi.org/10.1016/j.coal.2023.104433 (2024).
9. Han H. Comprehensive dust removal and dustproof technology in coal mine roadway excavation. *Energy Energy Conserv.* **07**, 168–170+174. https://doi.org/10.16643/j.cnki.14-1360/td.2024.07.076b (2024).
10. Xu, C. et al. Study on the deposition rates of inhaled dust in respiratory tract by anchor excavation driver during coal mining. *Adv. Powder Technol.* **35**(7), 104541. https://doi.org/10.1016/j.apt.2024.104541 (2024).
11. Du, T. et al. CFD modeling of coal dust migration in an 8.8-meter-high fully mechanized mining face. *Energy* **212**, 118616. https://doi.org/10.1016/j.energy.2020.118616 (2020).
12. Xu, C. et al. Numerical simulation of the effect of a wind-assisted spraying device during continuous mining. *Powder Technol.* **428**, 118803. https://doi.org/10.1016/j.powtec.2023.118803 (2023).
13. Lu, X. et al. The spatial diffusion rule and pollution region of disorganized dust in the excavation roadway at different roadheader cutting positions. *Powder Technol.* **396**, 167–180. https://doi.org/10.1016/j.powtec.2021.10.033 (2022).
14. Lyu, X. et al. Investigation and CFD simulation of coal dust explosion accident in confined space: A case study of Gaohe Coal Mine Ventilation Air Methane oxidation power plant. *Fire Saf. J.* **149**, 104237. https://doi.org/10.1016/j.firesaf.2024.104237 (2024).
15. Zhou, G. et al. Synthesis and performance characterization of a novel wetting cementing agent for dust control during conveyor transport in coal mines. *Powder Technol.* **360**, 165–176. https://doi.org/10.1016/j.powtec.2019.10.003 (2020).

16. Liu, Q. et al. Research on the control law of dust in the main ventilation system in excavated tunnels for cleaner production. *Build. Environ.* **205**, 108282. https://doi.org/10.1016/j.buildenv.2021.108282 (2021).
17. Liu, N. et al. Dust diffusion laws during partition excavation by boom-type roadheader in a metro tunnel. *Tunn. Undergr. Space Technol.* **141**, 105382. https://doi.org/10.1016/j.tust.2023.105382 (2023).
18. Hou, C. et al. Study on dust pollution characteristics and optimal dust control parameters during tunnel excavation by CFD simulation. *Adv. Powder Technol.* **34**(11), 104217. https://doi.org/10.1016/j.apt.2023.104217 (2023).
19. Nie, W. et al. Comparative study of dust pollution and air quality of tunnelling anchor integrated machine working face with different ventilation. *Tunn. Undergr. Space Technol.* **122**, 104377. https://doi.org/10.1016/j.tust.2022.104377 (2022).
20. Cao, Y. et al. Recent progress and perspectives on coal dust sources, transport, hazards, and controls in underground mines. *Process Saf. Environ. Prot.* https://doi.org/10.1016/j.psep.2024.04.095 (2024).
21. Wang, P., Lu, G. & Xu, Y. Research status and prospects of coal mine dust and prevention and control technology. *Mod. Min.* **39**, 8–13. https://doi.org/10.3969/j.issn.1674-6082.2023.11.003 (2023).
22. Yao, J. Exploration of coal mine dust prevention and control measures. *Energy Energy Conserv.* **05**, 145–147. https://doi.org/10.16643/j.cnki.14-1360/td.2024.05.059 (2024).
23. Hou, J. et al. Research and application of self-powered induction spray dust removal system for long-distance belt conveying in underground coal mines. *Process Saf. Environ. Prot.* **176**, 131–139. https://doi.org/10.1016/j.psep.2023.06.009 (2023).
24. Wang, J. Research progress on coal mine dust hazard and its prevention and control technology. *Coal Chem. Ind.* **52**, 53–56+72. https://doi.org/10.19889/j.cnki.10059598.2024.04.013 (2024).
25. Hu, S. et al. Characteristics of dust distributions and dust control measures around road-header drivers in mining excavation roadways. *Particuology* **58**, 268–275. https://doi.org/10.1016/j.partic.2021.03.017 (2021).
26. Nie, W. et al. Coupled diffusion law of windflow-gas-dust in tunnel energy extraction processes and the location of optimal pollution control exhaust duct. *Energy* https://doi.org/10.1016/j.energy.2024.132145 (2024).
27. Nie, W. et al. Study of spatiotemporal evolution of coupled airflow–gas–dust multi-field diffusion at low-gas tunnel. *Sci. Total Environ.* **928**, 172428. https://doi.org/10.1016/j.scitotenv.2024.172428 (2024).
28. Nie, W. et al. Distribution characteristics of an airflow–dust mixture and quantitative analysis of the dust absorption effect during tunnel sub-regional coal cutting. *Process Saf. Environ. Prot.* **164**, 319–334. https://doi.org/10.1016/j.psep.2022.05.068 (2022).
29. Zhou, G. et al. Study on coupling diffusion of composite dust and cloud-mist dedust technology in fully mechanized driving face of mixed coal-rock roadway. *Adv. Powder Technol.* **34**(1), 103911. https://doi.org/10.1016/j.apt.2022.103911 (2022).
30. Zhang, G. et al. Numerical simulation and engineering application of multistage atomization dustfall at a fully mechanized excavation face. *Tunn. Undergr. Space Technol.* **104**, 103540. https://doi.org/10.1016/j.tust.2020.103540 (2020).
31. Jing, D. et al. Research on the mechanism of multilayer spiral fog screen dust removal at the comprehensive excavation face. *PLoS One* **17**(4), e0266671. https://doi.org/10.1371/journal.pone.0266671 (2022).
32. John, J. et al. Computational fluid dynamics simulation of the turbulence models in the tested section on wind tunnel. *Ain Shams Eng. J.* **11**(4), 1201–1209. https://doi.org/10.1016/j.asej.2020.02.012 (2020).
33. Ren, S. et al. Research and development of vortex suction dedusting device based on multi-factor horizontal response surface method. *J. Clean. Prod.* **442**, 140916. https://doi.org/10.1016/j.jclepro.2024.140916 (2024).
34. Jing, D. et al. Numerical simulation and experimental study on dust suppression by supersonic spiral aerodynamic atomization. *J. Saf. Environ.* **23**, 4343–4350. https://doi.org/10.13637/j.issn.1009-6094.2022.2017 (2023).
35. Tong, L. et al. CFD-DEM numerical study on coal dust pollution law of coal transfer point in underground coal mine. *Saf. Coal Mines* **52**, 188–192+200. https://doi.org/10.13347/j.cnki.mkaq.2021.05.034 (2021).
36. Jiang, W. et al. Applying the similarity theory to model dust dispersion during coal-mine tunneling. *Process Saf. Environ. Prot.* **148**, 415–427. https://doi.org/10.1016/j.psep.2020.10.026 (2021).
37. Qiao, M. et al. Dispersion and migration characteristics of multisource respirable dust in development panels during tunnelling processes. *Tunn. Undergr. Space Technol.* **148**, 105778. https://doi.org/10.1016/j.tust.2024.105778 (2024).
38. Xiao, Y. et al. Diffusion characteristics of coal dust associated with different ventilation methods in underground excavation tunnel. *Process Saf. Environ. Prot.* **184**, 1177–1191. https://doi.org/10.1016/j.psep.2024.02.065 (2024).
39. Zhang, T. et al. Supersonic siphon suction water aerodynamic atomization in dust removal. *J. China Coal Soc.* **46**, 3912–3921. https://doi.org/10.13225/j.cnki.jccs.2021.0198 (2021).
40. Lou, J. et al. Research on multi-layer spiral spray dust removal technology in heading face. *Saf. Coal Mines* **55**, 94–99. https://doi.org/10.13347/j.cnki.mkaq.20221800 (2024).
41. Zhang, J. et al. Research on influence of different cutting positions in coal roadway on law of dust transport and diffusion. *Coal Technol.* **42**, 177–181. https://doi.org/10.13301/j.cnki.ct.2023.08.037 (2023).

Acknowledgements
This work has been funded by the National Special Support Plan for National Outstanding Youth Science Fund Project of National Natural Science Foundation of China (51704146), Natural Science Foundation of Liaoning Province (2020-MS-304), Scientific Research Fund of Liaoning Provincial Education Department (LJKZ0323), General Program of National Natural Science Foundation of China (52474229).

Author contributions
D.J. and K.Q. wrote the main manuscript text and C.P. proofread the manuscript . K.Q. and D.M. conducted numerical simulation calculations. M.J. and D.P. prepared Figs. 1, 2, 3, 4, 5, 6 and 7. D.M. and B.C. prepared Figs. 8, 9, 10, 11, 12, 13 and 14.

Declarations

Competing interests
The authors declare no competing interests.

Additional information
Correspondence and requests for materials should be addressed to M.D.

Reprints and permissions information is available at www.nature.com/reprints.

Publisher's note Springer Nature remains neutral with regard to jurisdictional claims in published maps and institutional affiliations.